Volume 1 | Number 1 | Jan 2013 | Pages 1–100

Journal of
Materials Chemistry A

Materials for energy and sustainability
www.rsc.org/materialsA

ROYAL SOCIETY
OF CHEMISTRY

ROYAL SOCIETY
OF **CHEMISTRY**

www.rsc.org/materialsA

Journal of Materials Chemistry A

COMMUNICATION

SnO₂ nano-rod with superior CO oxidation performance

Xiang Wang*, Lihong Xiao, Honggen Peng, Wenming Liu and Xianglan Xu

5 **SnO₂ nanoparticles with various morphologies were successfully prepared and characterized. Although SnO₂ nano-rod with preferentially exposed (110) crystal planes has the lowest surface area and lacks active oxygen species, it is the most active catalyst for CO oxidation, whose catalytic**
10 **behavior is similar to that of noble metal catalyst.**

The past two decades have witnessed significant progress in nanotechnology. The most interested research in this field was synthesis of new nanoparticles with different sizes and shapes and crystal structures. It has been found that the size and shape of

15 nanoparticles play crucial roles in the determination of physical and chemical properties[1]. For instance, for catalytic oxidation of 1,2-dichloroethane and ethyl acetate over various shapes of CeO₂, CeO₂ nano-rods showed the best catalytic activity, followed by nano-cubes and nano-octahedrons, respectively[2]. High surface

20 areas, exposition of the clearly defined crystal planes, and excellent mechanical properties are key factors that account for the enhanced catalytic performance, which can be tuned by varying the particle size and shape.[3] In another case, Xie et al.[4] utilized the calcination method to obtain Co₃O₄ nano-rods, which

25 showed an excellent catalytic property for CO oxidation attributing to the abundance of active Co³⁺ cations on (110) planes. Furthermore, nanoparticles with unique shapes can be used as key components for electronic devices. Therefore, shape-controlled synthesis of nanoparticles is an attractive research

30 field.

Tin(IV) dioxide is an important industrial chemical with a wide range of applications, which has been extensively studied as gas sensors[5], electrodes for photovoltaic devices[6] and anode material in lithium ion batteries[7]. Various novel nanostructures of tin

35 dioxide such as nano-rods[8], nanowires[9], nanobelts[10], nanotubes[11] and hollow sphere[12] have been successfully synthesized. Recent research has been focused not only on the development of shape-controlled synthesis, but also on the examination of their sensing, catalytic and surface properties. Han et al.[13] reported that SnO₂

40 exposed with (221) and (111) facets show enhanced catalytic activity and gas-sensing properties. Though SnO₂-based catalysts have been applied in CO Oxidation, the morphology and crystal plane effect on SnO₂ remain un-clear [14, 15].

Therefore, in this communication, single crystalline SnO₂

45 nano-rods, SnO₂ microspheres, SnO₂ nanoparticles (NPs) were synthesized by molten salt synthesis, traditional and hydrothermal methods and characterized by X-ray diffraction, transmission electron microscopy and X-ray photoelectron spectroscopy. Their

catalytic performances for CO oxidation were evaluated. SnO₂

50 with nano-rod morphology and the lowest surface area (1 m² g⁻¹) shows significantly efficient catalytic activity compared with other morphologies, and its catalytic behavior is very similar to that of the noble metal catalyst.
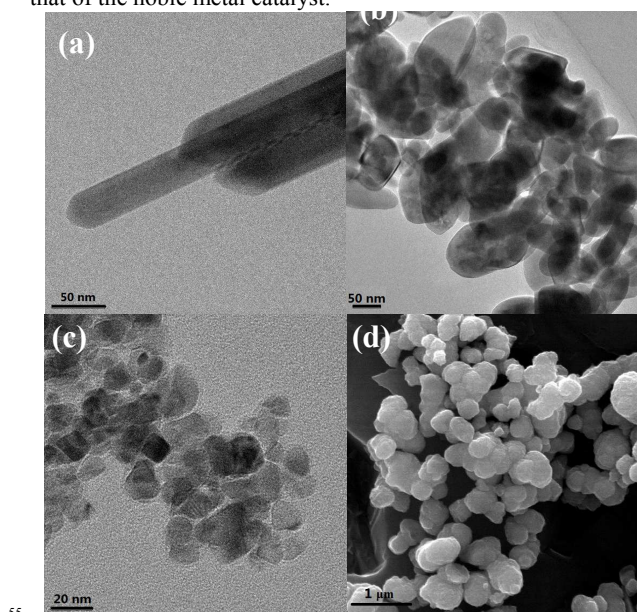

55 **Fig. 1** TEM images of SnO₂-Rod(a), SnO₂-NPh(**b**), SnO₂-NPp(c), and SEM images of SnO₂-Sphere(d).

Fig. 1 shows the typical TEM images of as-synthesized SnO₂ samples. SnO₂ nano-rods are structurally uniform, single

60 crystalline with a length of about 200-400 nm and an average diameter around 46 nm for width (**Fig. 1a**). Whereas **Fig. 1b** shows the TEM image of SnO₂ nanoparticles with an average size of around 30 nm. These nanoparticles are not uniformly structured and well-crystallized, thus without well-defined facets.

65 SnO₂ nanoparticles prepared by precipitation method are shown in **Fig. 1c**, which are irregular polyhedron and typically 12 nm in diameter. SnO₂ solid sphere with a diameter of 300-500 nm are shown in **Fig. 1d**.

As observed in **Fig. S1**, SnO₂-Sphere and SnO₂-Rod exhibit a

70 type I isotherm characteristic of microporous solids. Additionally, SnO₂-Sphere and SnO₂-Rod are characterized with an extremely low total pore volume and specific surface area, suggesting the nearly absence of pores, and are almost bulk. SnO₂-NPp showed a IV-type isotherm with a type H1 hysteresis loops indicating the

75 presence of mesopores. Type H1 hysteresis loops is often

associated with porous materials to consist of agglomerates or compacts of approximately uniform spheres, which is consistent with the TEM result. While SnO_2-NPh exhibited a type IV isotherm, which does not exhibit any limiting adsorption at high relative pressure (P/P_0) and hysteresis loops is type H_3. The BET surface area, average pore size and pore volume of the samples are listed in **Table 1**. From the **Table 1** we can also know that the agglomeration factor of SnO_2-Rod is approximately 1, which means that the SnO_2-Rod is indeed not aggregated[14]. In contrast, the agglomeration factor of SnO_2-Sphere is 54.5, indicating its severe agglomeration.
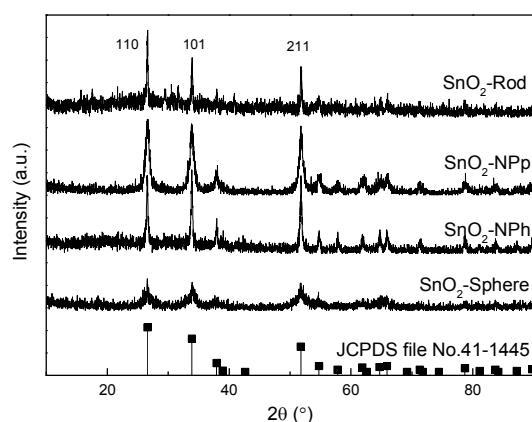

Fig. 2 XRD patterns of SnO_2 catalysts with various morphologies.

XRD patterns of the as-synthesized four samples are shown in **Fig. 2.** All the diffraction peaks are in good agreement with that of the standard pattern for pure tetragonal rutile SnO_2 (JCPDS card No. 041-1445). However, there are some differences among the shape of the diffraction peaks of these samples, which indicates the differences in the size, morphology and advantageous crystal facet. The sharp XRD peaks of SnO_2-Rod and SnO_2-NPh suggest their high crystallinity, while the peaks of SnO_2-NPp and SnO_2-Sphere are broadened with decreased intensity, indicating the decrease of crystalline. In addition, there are differences among the relative intensity of the XRD peaks of as-prepared samples, compared with the standard XRD pattern. The peak (110) of SnO_2-Rod is obviously stronger than other peaks, while other high-index facet is broader and weaker than that of the standard pattern.

Table 1 Textural parameter of SnO_2 with different morphologies

Sample	BET surface area (m^2/g)	Average pore size (nm) [a]	Pore volume (cm^3/g) [b]	Mean crystallite size (nm) [c]	Agglomeration factor[d]
SnO_2-Rod	1	14.9	0.003	46.3	1.0
SnO_2-NPp	25	8.6	0.086	11.5	1.4
SnO_2-NPh	9	25.6	0.056	29.3	1.6
SnO_2-Sphere	8	3.8	0.007	7.8	54.5

[a] Average pore size calculated from desorption branch. [b] The pore volume, measured at P/P_0=0.995. [c] The mean particle size is given in terms of particle cross-section (as obtained from SEM/TEM). [d] Agglomeration factor is the ratio of mean particle size (SEM/TEM) to the mean crystallite size (XRD).

The exposed crystal planes of SnO_2 with different shapes are

further investigated by HRTEM and presented in **Fig. S2.** The HRTEM images clearly show the expose facets of the SnO_2 nanostructures. The lattice fringes with spacing of 0.334 nm and 0.177 correspond to the (110) and (211) plane of rutile SnO_2 respectively. As shown in **Fig. S2a,** the outer surface of SnO_2-Rod is enclosed by clear and well-defined (110) planes. The exposure facet of SnO_2-NPh and SnO_2-NPp is similar, (110) and (211) plane can be observed on the surface. Very different from SnO_2-NPh and SnO_2-NPp, SnO_2-Sphere only show few (110) plane exposed on the surface of microsphere.

The surface chemical composition of the as-prepared SnO_2 was further characterized by X-ray photoelectron spectroscopy (XPS) analysis. The peaks at about 495 eV and 486 eV were attributed to $Sn3d_{3/2}$ and $Sn3d_{5/2}$ of Sn^{4+}, respectively. Integrated peak areas of the Sn3d and O1s cores were measured and used to calculate the chemical compositions of the samples. Areas were determined by fitting the curves using a nonlinear least squares curve fitting program (Origin). The atomic ration of Sn/O is nearly 1/2. Clearly, these results prove that the sample is single SnO_2 with rutile structure. This is consistent with the above-mentioned XRD results. From **Fig. S3**, it showed that O1s XPS was asymmetric, indicating that at least two oxygen species were presented in the nearby region. The peak at about 530 eV is due to oxygen species in the SnO_2 crystal lattice (the standard binding energy for O crystal lattice is 530.6 eV), which corresponds to O-Sn bonds.

H_2-TPR profiles of the samples are shown in **Fig. S4**. SnO_2-Rod shows only a small reduction peak at 400~800 °C, indicating its lack of reducible and active oxygen species. While other three samples exhibit a major reduction peak in the temperature region from 450 to 780 °C, which is ascribed to the reduction of SnO_2 to metallic Sn. The quantification results revealed an O/Sn atomic ratio around 2/1 for SnO_2-NPh, SnO_2-NPp, and SnO_2-Sphere, which is consistent with the stoichiometry of SnO_2 formula. The O/Sn atomic ratio of SnO_2-Rod is around 1/5 suggests that only 10% of SnO_2-Rod is reduced. This may ascribe to that the SnO_2-Rod has a larger crystalline size with clear and smooth (110) surfaces covered, which have the lowest surface energy[16]. Thus SnO_2-Rod required high temperature to be totally reduced.
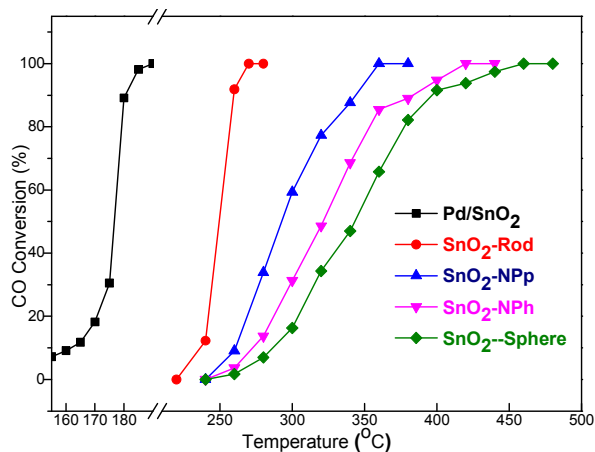

Fig. 3 Catalytic performance of Pd/SnO_2 and SnO_2 with various morphologies for CO oxidation.

It is well-known that the surface and crystal structure of materials greatly affect the catalytic activity. To investigate the

surface effect on catalytic properties of SnO_2, the catalytic oxidation of CO were chosen as the probe reaction. **Fig. 3** shows the relationship between CO conversion and temperature with the as-prepared SnO_2 nanoparticles as catalysts. SnO_2-Rod exhibited the best catalytic activity and reached 100% conversion at 260 °C. Meanwhile, the 100% conversion temperature for SnO_2-NPh, SnO_2-NPp and SnO_2–Sphere are much higher than the aforementioned SnO_2-Rod, namely at 360, 420 and 460 °C, respectively. It should be noted that the catalytic behavior of SnO_2-Rod is, among all SnO_2 samples studied, mostly approaching the behavior of noble metal catalysts (**Fig. 3**, Pd/SnO_2 and the HRTEM images in **Fig. S6**), which generally has a light-off curve at relatively low reaction temperature (~180 °C).

Generally, catalysts with higher BET surface area often lead to higher catalytic activities. For instance, Xie's group[15] reported that SnO_2 nanosheet with a 5 atom layer thickness and also with a high surface area (173.4 m^2 g^{-1}) shows the best catalytic activity for CO oxidation. However, in our work, the order of BET surface area of four samples is not consistent with the order of activity. As shown in **Table 1**, the BET surface areas of the samples are 1, 25, 9 and 8 m^2/g for SnO_2-Rod, SnO_2-NPp, SnO_2-NPh and SnO_2-Sphere, respectively. SnO_2-Rod with the lowest surface area presented the best catalytic activity among the samples. SnO_2-NPh and SnO_2-Sphere have similar specific surface areas while showed obviously differences in CO oxidation activity.

The catalytic activity of the nanoparticles are largely determined by the energy of surface atoms, which can be easily gauged by the number of neighboring atoms, and by the bonding modes and accompanying energies of small molecules to be transformed on the nanoparticle surface. The inherent surface energy of the crystal facets would determine the overall reactivity of the catalytic surface of interest[17].

Usually, for CO catalytic oxidation over SnO_2, the reaction proceeded via a Mars-Van Krevelen mechanism[18]. CO is adsorbed on a surface Sn active site firstly and then oxidized by the surrounding less coordinated O atom, leading to oxygen vacancy creation; after that, gas-phase O_2 would react with the reduced surface to regenerate the surface oxygen atom. The tendency for adsorbing CO molecule and losing one oxygen atom to carbon monoxide from SnO_2 should be an important factor in determining how good a SnO_2 catalyst is. It is well known that there are different planes in the crystal structure, on which the densities of the Sn atom are different. This causes the energy required from the adsorption features for CO and create oxygen vacancies differently. A catalyst exposed planes of more Sn atom could provide more unsaturated-coordinated sites which are more active to interact with CO and have higher catalytic activities. From the analysis of the HRTEM and XRD, we have obtained SnO_2-Rod with (110) planes preferentially exposed. This could be a chief reason leading to its extra high CO oxidation activity which is similar to the noble metal catalysts. However, the real mechanism of CO oxidation over SnO_2 nano-rod is still needed to be further studied. This is because the catalytic behavior and H_2-TPR of SnO_2 nano-rod is very different from the SnO_2-NPp, SnO_2-NPh and SnO_2-Sphere.

The stability test result of CO oxidation over SnO_2-Rod was shown in **Fig. S5**. After running at 260 °C for 100 h, the conversions of CO over the SnO_2-Rod were almost maintained. This indicated that the redox features of the SnO_2 nano-rod were quite stable under the CO oxidation atmosphere.

In summary, SnO_2 catalysts of various morphologies were successfully prepared by molten salt synthesis, chemical precipitation and hydrothermal synthesis methods. The SnO_2 nano-rods showed the best catalytic activity for CO oxidation among the four different morphologies of SnO_2. The catalytic behavior of SnO_2-Rod is similar to the noble metal catalysts, which can reduce the catalyst cost and reducing the using of noble metals. It is evident that the nanostructures of catalysts are very important to their catalytic performance. The specific exposure crystal planes with relative higher density of Sn atoms, e.g. (110), impact the catalytic performance very significantly although traditional point indicates that the catalytic properties strongly depend on the BET surface area. The more well-defined reactive plane (110) generated, the higher CO oxidation activity is shown. The present results suggest that specifically designed nano-materials with predictable morphologies and preferential exposed crystal planes by controlling synthesis parameters might bring new opportunities for developing novel high performance catalysts. It is expected that, a more efficient SnO_2 nanorod will be developed by further improving the surface area and effectively controlling the growth of nano-crystal and the elongation direction.

Notes and references

[a] *999 Xuefu Road, Honggutan New District, Department of Chemistry, Nanchang University, Nanchang, P. R. China. Fax: +86 0791-3969064;Tel: +86 0791-3969064, E-mail: xwang23@ncu.edu.cn*

† Electronic supplementary information (ESI) available: Details of catalyst preparation and characterization. See DOI: 10.1039/b000000x/

1. C. Burda, X. Chen, R. Narayanan and M. A. El-Sayed, *Chem. Rev.*, 2005, **105**, 1025.
2. H. X. Mai, L. D. Sun, Y. W. Zhang, R. Si, W. Feng, H. P. Zhang, H. C. Liu and C. H. Yan, *J Phys. Chem. B*, 2005, **109**, 24380.
3. R. Krahne, L. Manna, G. Morello, A. Figuerola, C. George and S. Deka, *Phys. Part. Nucl.*, 2013, **1**.
4. X. Xie, Y. Li, Z. Q. Liu, M. Haruta and W. Shen, *Nature*, 2009, **458**, 746-749.
5. T. Wagner, C.-D. Kohl, M. Fröba and M. Tiemann, *Sensors*, 2006, **6**, 318.
6. H. Kim, G. P. Kushto, R. C. Y. Auyeung and A. Piqué, *Appl.Phys. A*, 2008, **93**, 521.
7. Z. Wang, D. Luan, F. Y. Boey and X. W. Lou, *J. Am. Chem. Soc.*, 2011, **133**, 4738.
8. Yingkai Liua, Chenglin Zhenga, Wenzhong Wanga, YongjieZhana and G. Wanga, *J. Cryst. Growth*, 2001, **233**, 8.
9. Y. D. Ko, J. G. Kang, J. G. Park, S. Lee and D. W. Kim, *Nanotechnology*, 2009, **20**, 455701.
10. J. Duan, S. Yang, H. Liu, J. Gong, H. Huang, X. Zhao, R. Zhang and Y. Du, *J. Am. Chem. Soc.*, 2005, **127**, 6180.
11. J. Ye, H. Zhang, R. Yang, X. Li and L. Qi, *Small*, 2010, **6**, 296.
12. Y. Q. Guo, Y. Li, R. Q. Tan and W. J. Song, *Mater. Sci. Eng. B*, 2010, **171**, 20.
13. X. Wang, X. Han, S. Xie, Q. Kuang, Y. Jiang, S. Zhang, X. Mu, G. Chen, Z. Xie and L. Zheng, *Chemistry*, 2012, **18**, 2283.
14. J. Yu, D. Zhao, X. Xu, X. Wang and N. Zhang, *ChemCatChem*, 2012, **4**, 1122-1132.

15. Y. Sun, F. Lei, S. Gao, B. Pan, J. Zhou and Y. Xie, *Angew.Chem. Int. Ed.*, 2013, **52**, 10569-10572.

16. J. Oviedo and M. J. Gillan, *Surface Science*, 2000, **463**, 93.

17. K. Lee, M. Kim and H. Kim, *J. Mate. Chem.*, 2010, **20**, 3791.

5 18. M. Batzill and U. Diebold, *Prog. Surf. Sci.*, 2005, **79**, 47.